

Charting 5G Energy Efficiency: Flexible Energy Modeling for Sustainable Networks

Anderson L. de Araujo*, Luc Deneire*, Guillaume Urvoy-Keller *, André L. F. de Almeida†

*Université Côte d’Azur, I3S, Sophia Antipolis, France

†Department of Teleinformatics Engineering, UFC, Fortaleza, Brazil

Abstract—Despite the rapid advancements in 5G technology, accurately assessing the energy consumption of its Radio Access Networks (RANs) remains a challenge due to the diverse range of applicable technologies and implementation solutions. To estimate the energy consumption in 5G networks, this study proposes a new method to model the energy of the baseband of the RANs, along with an end-to-end model inspired by the literature. The objective is to design a versatile energy model capable of estimating RAN-specific energy consumption, encompassing both mobile terminals and the physical layer (PHY) of base stations. The core of the model lies in the estimation of the number of operations done by PHY-layer algorithms. This method is compared with the estimation of the number of cycles (and energy per cycle) used by a specific implementation (here a Matlab code ported on an Intel target). This enables to assess the model with the estimation of energy consumed on a real target. Overall, the results highlight the need for improved modeling techniques to better match the energy consumption patterns observed in the simulations. The main contribution of this study is a first step towards a flexible energy model with smaller granularity that can be used to compare the energy used for multiple applications and in different contexts, providing a comprehensive tool for assessing and optimizing 5G network energy consumption.

Index Terms—5G networks, energy consumption, Radio Access Network (RAN), energy model, 5G New Radio (NR)

I. INTRODUCTION

Over the past decade, the mobile communication sector has witnessed remarkable growth, fueled by the increasing demand for data traffic and services [1]. This surge in activity has led to a corresponding rise in energy consumption. Mobile networks typically consist of the Radio Access Network (RAN), which includes user equipment (UE) and base stations (BS), along with the network core. Notably, BSs can account for up to 80% of the energy consumption in mobile networks’ operational expenditure (OPEX) [2]. Consequently, academia and industry have made concerted efforts to develop more environmentally friendly mobile networks.

Research efforts have focused on developing power models for base stations (BS) due to their significant energy consumption ([3] and [4] present models based on 4G networks). In ”How much energy is needed to run a wireless network?” [3], the BS is broken down into its constituent components: baseband unit (BBU), radio frequency (RF), power amplifier (PA), and overhead (OH, related to cooling and power supply). Desset et al. [4] further refine this model by dissecting the BBU and RF components into subcomponents and incorporating their operations as model inputs. Yan et al. [5] introduce a model to estimate energy consumption for mobile services

based on different application types. By characterizing mobile services according to network topology segments, the authors estimate energy consumption for each part of the topology (user equipment (UE), base station (BS), wireline core, and data center (DC)) to determine the total energy consumed during mobile service usage.

The development of the latest mobile generation, driven by the need for higher throughput and lower latency, prioritized ultra-lean design principles, to minimize non-data-related transmissions. This led to the creation of 5G New Radio (NR), aimed at improving energy efficiency compared to 4G Long Term Evolution (LTE). The survey by López-Pérez et al. [6] explores the current state of research on 5G energy efficiency. They review various power consumption models for distributed and centralized Radio Access Network (RAN) architectures and discuss key energy efficiency technologies, highlighting their benefits and challenges through detailed examinations of implementations and operational aspects.

Williams et al. [7] point out gaps in studies related to 5G energy consumption, emphasizing the need for openly accessible, vetted, and transparent assessments of the entire network. They underscore the importance of considering not only direct energy savings but also indirect and rebound effects when evaluating 5G’s energy-saving potential.

Larsen et al. [8] gather research efforts aimed at minimizing the energy consumption of future mobile networks. They explore various approaches, such as RAN architecture enhancements, technological improvements, and network sharing among operators. The authors discuss the feasibility of these approaches in real-world scenarios, highlight their current state of development, and propose guidelines to promote the environmental sustainability of NR and subsequent mobile generations.

Regarding 5G (NR), several studies have investigated its energy and power consumption. Xu et al. [9] and Narayanan et al. [10] examined the power consumption of UEs, smartphones, when using 5G networks compared to 4G LTE. Tombaz et al. [11] evaluated the power consumption of a 5G system incorporating massive beamforming and ultra-lean design principles, employing a power model based on resource utilization. Yu et al. [12] addressed an energy-efficient resource allocation problem for joint downlink and uplink transmission with Carrier Aggregation (CA) through optimization techniques. Fu et al. [13] adapted a power model originally described by Desset et al. [4] for 5G BSs, next generation Node Bs

(gNBs), along with the power consumption of Light-Fidelity (Li-Fi) technologies and millimeter wave (mmWave) indoor access points (IAPs) and their respective power consumption levels.

Additionally, given the diverse range of technologies applicable to 5G and the various implementation solutions available, conducting a robust energy assessment of the Radio Access Network (RAN) through a power model requires extensive data collection and experimental studies to accurately identify the relevant parameters specific to real-world 5G equipment. Thus, the question is : is it possible to design a versatile power model to capture the range of technologies applied to 5G to estimate the RAN specific power consumption encompassing both the mobile terminal and the PHY part of the base station?

The objective of this study is to contribute to the development (and to enhance) of an end-to-end energy/power model to estimate the amount of power consumed when using 5G networks. The model is based on the algorithms and protocols used by the 5G NR physical layer (PHY-layer) and their costs per operation. The core of the model involves estimating the number of operations performed by PHY-layer protocols in both base stations and user equipment. Overall, the results highlight the need for improved modeling techniques to better match the energy consumption patterns observed in the simulations, such as the adoption of optimized matrix multiplication algorithms. The model itself is compared to energy estimation on a real target (here an Intel target with code generated by Matlab). The main contribution of this study is a first step to a flexible energy model with smaller granularity that can be extended for multiple applications and different contexts, providing a comprehensive tool for assessing 5G network energy consumption.

The outline of the paper is as follows. Section II introduces the related works done before. The model and simulation parameters are presented in Section III. The results are presented and discussed in Section IV. Finally, Section V concludes the paper.

II. RELATED WORKS

In this section we highlight pertinent studies that have contributed to the state of the art and understanding of power consumption modeling of the RAN. By synthesizing the current state of knowledge, we aim to highlight gaps, identify areas of consensus, and delineate the unique contributions of our work.

In the early 2010s, the Energy Aware Radio and Network Technologies (EARTH) project (Auer et al. [3]) analyzed the power consumption of BS by breaking it down into components such as BBU, RF, PA, and OH. They found a linear relationship between the power consumption and the number of transceivers N_{TRX} , as well as the load level of the BS. This relationship was quantified in (1), where P_{in} represents the power consumed by the BS, P_0 is the power consumed by a transceiver at minimum non-zero output power, P_{sleep} denotes the power consumed in sleep mode by a transceiver,

P_{out} stands for the output power from the transceiver, and Δ_p represents the load-dependent slope.

$$P_{in} = \begin{cases} N_{TRX} (P_0 + \Delta_p P_{out}), & \text{if } 0 < P_{out} < P_{max} \\ N_{TRX} P_{sleep}, & \text{if } P_{out} = 0 \end{cases} \quad (1)$$

In [4], the EARTH project went deeper on the power breakdown of the BS components stated in (2), specially regarding the BBU and RF, where the authors defined a dependency on the components and operations within these unities.

$$P_{BS} = P_{BBU} + P_{RF} + P_{PA} + P_{OH} \quad (2)$$

Yan et al. [5] assessed the RAN energy consumption by modeling the LTE energy consumption by the sum of the segments of the network, such as the UE, BS, wireline core, that connects the RAN to datacenters, and DC, as in (3).

$$E_{total} = E_{UE} + E_{BS} + E_{wireline} + E_{DC} \quad (3)$$

Regarding the BS energy consumption, denoted by E_{BS} , it is established a dependency on the number of resource elements used for data transmissions and control signaling.

In [12], the authors developed a model for the power consumption of a 5G system incorporating CA. They found that the power consumed at the BS consists of both static and dynamic components, both of which are influenced by the system's load level. The model, described in (4), considers parameters such as P_{TX_j} , $P_{CP_j}^{CA}$, and P_{CP}^{CAi} , representing the effective transmit power consumed by the j -th component carrier (CC), the variable and static power consumed by shared hardware components across CCs, respectively. Additionally, N_{CC} and B_j denote the number of CCs and the bandwidth of the j -th CC.

$$P_{BS} = \sum_{j=1}^{N_{CC}} (P_{TX_j} + B_j P_{CP_j}^{CA}) + P_{CP}^{CAi} \quad (4)$$

Regarding [11], the authors design a power model for 5G systems while incorporating massive Multiple Input Multiple Output (mMIMO) on the link budget. The power consumed at the BS, described in (5), is proportional to the number of sectors N_s in the BS, and encompasses three scenarios: i) during transmission, including the transmit power per sector P_{tx}^s adjusted by the PA energy efficiency η_{PA} , the number of RF chains N and the additional digital and RF processing per antenna P_C , along the baseline power consumption of each sector P_B ; ii) in the absence of transmission, and no cell discontinuous transmission (DTX), then only the baseline power consumption is accounted; iii) in the absence of transmission, but cell DTX is implemented, the the power consumed by the sector is a fraction of the baseline power, defined by the cell DTX factor δ .

$$P_{BS} = N_s \times \begin{cases} \frac{P_{tx}^s}{\eta_{PA}} + NP_C + P_B, & \text{if } P_{tx}^s > 0 \\ P_B, & \text{if } P_{tx}^s = 0, \text{ no DTX} \\ \delta P_B, & \text{if } P_{tx}^s = 0, \text{ and DTX} \end{cases} \quad (5)$$

Fu et al. [13] tailored a power model based on 2 where the BS was composed of multiple nodes. For each node, the BBU and the RF power consumption is a function of the operation complexity, Q measured by Giga floating-point operations per second (GFO/S), for operations within these components, adjusted by the technology-dependent factor ρ , measured in Giga floating-point operations per Watt (GOP/W). The BBU power consumption is described generically in 6, where is presented the encoding, network and control operations, and the power consumed is a function of the number of beamforming L . The RF power consumption is described in a similar way, in (7), but with the operations within the RF, such as modulation, mixer, variable gain amplifier (VGA), low-noise amplifier (LNA), ADC and clock, and proportional to the number of antenna elements M .

$$P_{BB} = L(Q_{enc} + Q_{net} + Q_{ctrl})/\rho \quad (6)$$

$$P_{RF} = M(Q_{mod} + Q_{mix} + Q_{vga} + Q_{lna} + Q_{adc})/\rho + \sqrt{M}Q_{clk}/\rho \quad (7)$$

III. METHOD

In this section, we develop the energy model, inspired by [13]. It is based on the algorithms and protocols used by the NR PHY-layer, depicted on the Third Generation Partnership Project (3GPP) technical specifications, and their costs per operation. The core is the estimation of the number of operations and the number of CPU cycles at the BBU, generated from the protocols from the PHY-layer downlink BS and the UE and, from that, calculate the energy consumed for transmission for a given scenario.

The model is composed by eight blocks, each one is a group of algorithms done for the processing of the signal. On the BS side, there are: cyclic redundancy check (CRC) attachment, code block (CB) segmentation and CRC attachment, channel coding, rate matching, in block A; CB concatenation, scrambling, modulation, layer mapping, in block B; antenna port mapping, mapping to virtual resource block (VRB), mapping from VRB to Physical Resource Block (PRB), in block C; Orthogonal Frequency-Division Multiplexing (OFDM), and Cyclic Prefix (CP) addition, in block D. On the UE side, there are CP remove, OFDM demodulation, in block E; channel estimation, in block F; layer demapping, descrambling, in block G; and rate recovery, channel decoding, desegmentation, and CRC decoding in block H. The notation \mathcal{O} represents the number of operations estimated by the model. It is assumed that the addition and operations for memory vectors have the same cost in terms of micro-operation (μop) for the matrix

inversion, for the Least Squares (LS) estimation, the Single Value Decomposition (SVD) and the fast Fourier transform (FFT) used to compute the discrete Fourier transform (DFT) algorithms, .

The validation of this model is done by comparison with a MATLAB simulation, where the NR PHY-layer is implemented using the 5G toolbox. The system on a chip (SoC) Blockset toolbox in MATLAB is used to get the number of operations at each one of the Blocks described in this section, from a `xlsx` file generated by it. The main inputs of this simulation are the number of slots, the desired signal-to-noise ratio (SNR), the modulation, the code rate, the subcarrier spacing, the gridsize, and the number of antennas at the transmitter and at the receiver.

Once the operations are quantified and sorted into the different types, the next step is to map them into assembly instructions, to go into a lower level on the CPU processor and quantify the number of cycles necessary to perform those operations. Fog [14] presents a mapping from the assembly instructions and the number of cycles needed to perform the required operation in a specific type of memory operand, used for both model and simulation. Then, once the total number of cycles is acquired, the total energy consumed is proportional to the number of cycles. The energy consumed per cycle ϵ , as used in Hao et al. [15] and described in (8), depends on the squared clock frequency of the processor f_{pc} , and an energy coefficient κ .

$$\epsilon = \kappa f_{pc}^2 \quad (8)$$

A. Block A

The most relevant algorithms, in terms of the number of operations, are the CRC attachment, CB segmentation and CRC attachment, and channel coding. The base graph selection, rate matching, and CB concatenation do not contribute significantly compared to these algorithms. The operations for CRC attachment depend on the input size. Let A be the number of input bits. In each iteration of the CRC algorithm using the slice-by-4 method, p bits are read per step. The number of AND, XOR, and shift operations are performed equally, as described in (9). For CB segmentation and CRC attachment, the segmentation requires nine operations per transport block (TB), and the CRC attachment is done for each CB. The total number of operations, for all the CRCs calculation for the CBs, is approximated to the sum of all CB sizes. If the TB size is A , the sum of all CB sizes B is defined as $B = A + LC$, where L is the CRC prefix and C is the number of CBs.

$$\mathcal{O}_{crc} = 5 \left\lceil \frac{A}{p} \right\rceil + 1 \quad (9)$$

Regarding channel coding for the data channel, the low-density parity check (LDPC) algorithm is applied for each CB. Let K , $Z_{i,j}$, n_1 , N_{BG} , M_{BG} , and N_{cCB} be the maximum CB size, the LDPC lifting size, the number of non-null elements in a base-graph matrix, the number of rows, and the number

of columns in a base-graph matrix, and the size of the coded CB, defined by the technical specifications, respectively.

The process, for each CB, is depicted into validation of non-null input bits, described in (10), replacements on the base graph matrix, described in (11), the calculation of the modulo operator, which has the cost of a division operation, described in (12) a large matrix product, described in (13), and setting of values into the output CB, described in (14). The total number of instructions generated by the channel coding is equal to the sum of the instructions from (10) to (14) times the number of CBs C .

$$\mathcal{O}_{LDPC-val} = 2(K - 2Z_{i,j}) \quad (10)$$

$$\mathcal{O}_{LDPC-rep} = N_{BG} \cdot M_{BG} \quad (11)$$

$$\mathcal{O}_{LDPC-n1} = n_1 \quad (12)$$

$$\mathcal{O}_{LDPC-mp} = N_{BG} \cdot Z_{i,j} (2M_{BG} \cdot Z_{i,j} - 1) \quad (13)$$

$$\mathcal{O}_{LDPC-set} = N_{cCB} + 2Z_{i,j} - K \quad (14)$$

B. Block B

In this block, three procedures are applied to each TB (also named codeword): scrambling, modulation and layer mapping. Scrambling: This involves an XOR operation between the codeword of size M_{cw} and a scrambling sequence of the same size. The scrambling sequence is generated using 5 XOR operations, resulting in a total of $6M_{cw}$ XOR operations for scrambling, in (15). Modulation: Performed at the RF level, and so, not entirely taken in account by this model, this is considered a generic operation, such as a table look-up for each modulation symbol, in (16). Layer Mapping: This involves shifting the modulated symbols into the layers available for transmission, requiring $N_{symbols}$ shift operations.

$$\mathcal{O}_{scmb} = 6M_{cw} \quad (15)$$

$$\mathcal{O}_{mod} = N_{symbols} \quad (16)$$

C. Block C

In this block, the main step is the antenna port mapping (APM), where the precoding is done based on the channel state information (CSI) report, as well as the mapping from the v layers to the P antenna ports indicated by the CSI report. The steps mapping to VRB and mapping from VRB to physical resource block (PRB) can be omitted since the operations done here are small compared to the APM. The APM can be resumed in the calculation of the precoding matrix by the application of the SVD on the information present on the CSI report, and the matrix multiplication of the precoding matrix and the block of vectors $[x^{(0)}(i), \dots, x^{(v-1)}(i)]^T, i = 0, 1, \dots, M_{symp}^{layer} - 1$, where $M_{symp}^{layer} = N_{symbols}/v$. The precoding matrix has dimensions $P \times v$, and each Block of vectors has dimensions $v \times 1$.

The SVD of a matrix with dimensions $m \times n$, has a around $2mn^2 + n^3 + n + mn$ floating-point operations (FLOPs). Then, this block, has a total of $2Pv^2 + v^3 + v + Pv$ FLOPs from

the SVD calculation, and $2Pv - P$ FLOPs from the matrix calculation, per M_{symp}^{layer} , resumed in (17).

$$\mathcal{O}_{apm} = M_{symp}^{layer} (2Pv^2 + v^3 + v + Pv + 2Pv - P) \quad (17)$$

D. Blocks D and E

The Blocks D and E are described together as Block D represents the OFDM modulation and CP addition, while Block E represents the reverse operations, OFDM demodulation and CP remove. As the CP related operations are not significant compared to the OFDM (de)modulation, they are not taken in account.

The modulation is done by the inverse Fourier Fast Transform (IFFT) application at the transmitter side on the resource grid of dimensions $N_f \times g \times N_{Tx}$, where f, g , and N_{Tx} are the number of subcarriers, the number of OFDM symbols and the number of transmit antennas. While the demodulation is done by the FFT application on the received signal at the receiver side to recover the same grid. The number of operations done in this step is defined by the application of the Radix-2 (i)FFT algorithm, with FFT size equal to N_{FFT} . It leads to the number of operations in (18), where $N_{FFT} > N_f$. As Block E is the inverse operation, FFT, the number of operations are the same.

$$\mathcal{O}_{FFT} = 5gN_{Tx}N_{FFT} \log_2 N_{FFT} \quad (18)$$

E. Block F

This block is responsible for the channel estimation on the UE side, where the channel is estimated by using the pilot symbols and LS estimation, and Minimum Mean Squared Error (MMSE) equalization is applied to data symbols.

Inspired by [16], the channel estimation by the LS method, per reference signal port (the same as layers for Block C) and per receiver antenna is obtained by the product of the pseudo-inverse of the pilot training symbols matrix and the received signal at the receive antenna. Let L, g, f and f_p be the maximum channel length, the number of OFDM symbols in a slot, the total number of OFDM subcarriers and the OFDM subcarriers with pilots. To obtain the pseudo-inverse of $\tilde{A} \in \mathbb{C}^{gf_p \times LN_t}$, the matrix composed by the pilot sequences, it is necessary to perform a matrix product, followed by a matrix inversion, and a last matrix product. The first matrix product has $(LN_t)^2(2gK_p - 1)$, the inversion operation, using the LU decomposition, has $(LN_t)^3$ operations, and the final matrix product has $(gK_p LN_t)(2LN_t - 1)$ operations. The estimation of the N_r channels perceived by the v reference signals, each one experienced by a receiver antenna, leads to (19).

$$\mathcal{O}_{LS} = vN_r [(LN_t)^2(2gK_p - 1) + (LN_t)^3 + (gK_p LN_t)(2LN_t - 1)] \quad (19)$$

Regarding the equalization, the MMSE algorithm, its operations are dominated by the SVD calculation of the channel matrix, and the application of that equalization, for each subcarrier. Consider the system described in (20), where $Y(f)$

and $Z(f) \in \mathbb{C}^{N_r \times g}$, $H(f) \in \mathbb{C}^{N_r \times N_t}$, and $X(f) \in \mathbb{C}^{N_t \times g}$ are, respectively the received signal and the noise at subcarrier f , the channel matrix and the transmitted symbols at subcarrier f . The svd of $H(f)$ leads to $2(N_r)(N_t)^2 + (N_t)^3 + N_r + N_r N_t$ FLOPs per subcarrier.

$$Y(f) = H(f)X(f) + \eta(f) \quad (20)$$

Given the SVD of $H(f) = U(f)\Sigma(f)V^H(f)$, where $U(f) \in \mathbb{C}^{N_r \times N_r}$, $\Sigma(f) \in \mathbb{R}^{N_r \times N_t}$ and $V(f) \in \mathbb{C}^{N_r \times N_t}$, the equalized symbols is described in (21), where $\Xi = [\Psi_{N_t \times N_t} \quad 0_{(N_r - N_t) \times N_t}]^T$ and Ψ is described in (22), where σ_n^2 is the noise variance, and $\sigma_i, i = 1, \dots, N_t$ is the i -th singular value in $\Sigma(f)$.

$$\hat{X}(f) = V(f)\Xi(f)U^H(f)Y(f) \quad (21)$$

$$\Psi = \text{diag} \left(\frac{\sigma_i(f)}{\sigma_i^2(f) + \sigma_n^2(f)} \right) \quad (22)$$

For each subcarrier, the construction of Ψ requires 3 operations to be done per singular value, and there are 3 matrices multiplications with $N_t N_r (2N_t - 1)$, $N_t N_r (2N_r - 1)$, and $N_t g (2N_r - 1)$ operations, respectively, leading to (23) total operations.

$$\begin{aligned} \mathcal{O}_{eq} = & 2N_r N_t^2 + N_r^3 + N_r + N_r N_t + N_f [3N_t \\ & + N_t N_r (2N_t - 1) + N_t N_r (2N_r - 1) + N_t g (2N_r - 1)] \end{aligned} \quad (23)$$

F. Block G

This block is the reverse block of block B, and so the operations here are the inverse of the ones done at block B: layer demapping, symbol demodulation, and symbol descrambling. The number of operations done in this block is described by (15) and (16), as well.

G. Block H

The last block is composed by the rate recovery, channel decoding, desegmentation, and CRC decoding, where the most relevant operations come from the LDPC decoding, desegmentation, where a CRC decoding is done over the CBs and a final CRC decoding done over the TB.

Regarding the LDPC decoding, it is done by a message passing algorithm and using log-likelihood ratios (LLRs), and the Min-Sum algorithm. Let N , W , $|\mathcal{N}(w)|$, and $|\mathcal{W}(n)|$ be, respectively, the number of variable nodes (i.e., the number of bits on the coded CB), the number of check nodes (i.e., the number of redundancy bits added at the encoding), the number of variable nodes connected to the check node w , and the number of check nodes connected to variable node n . The decoding process is done in four steps: initialization, done at the beginning of decoding with N quotients and N log calculations; horizontal step, done once per iteration, with $w|\mathcal{N}(w)|$ products; vertical step, done once per iteration, with $N|\mathcal{W}(n)|$ additions; and decision step, done once per

iteration, with $N(|\mathcal{W}(n)| + 1)$ additions and $\sum_{w=1}^W |\mathcal{N}(w)|$ XOR products.

Similarly to the BS side, the CRC decoding is done for the TB and for the CB. It is done by a comparison between the received CRC header and a new header computed at the receiver, using the received TB. If they are equal, then, the data is not corrupted, otherwise, there is a failure during transmission. Hence, the number of operations (AND, XOR and shifts) done at the decoding for TB and CBs is equal to the number of operations done at the encoding, plus the comparison.

IV. RESULTS AND DISCUSSION

In this section we present the findings of the study to develop a 5G NR end-to-end energy model based on the PHY-layer-layer protocols and algorithms. The model results are under the tag Model, while the validation results are under the tag Measurements.

During the simulation, functions other than the ones at the 5G and Communications System toolboxes are used, such as auxiliary functions for code generation. The file obtained from the simulation is composed by three reports per function analyzed. One is the Path aggregated report, used to identify the desired toolboxes for measurements, other is the Operator aggregated report, not used in this validation, and the last one is the Operator detailed report, where the information necessary for validation is obtained.

The reports are processed using the `pandas` library from python. First, the MATLAB auxiliary functions are excluded to avoid noise in the energy estimation, by filtering the data present on the Path aggregated report. Then, the Operator detailed report is used to get the necessary information for the estimation, including data type, operation, and count of operations. There are mainly seven types of data: logical, int32, and double (which means a double precision floating point), in both scalar and vector flavours, and struct as well. The operators are translated into assembly instructions and then into μ ops using the data from [14] (data updated in 2022), based on the type of memory used. It is assumed that scalars are stored in register operands and vectors are stored in memory operands (logical and integer vector are assumed to be stored in mmx registers, and double vectors to be stored in xmm registers).

The parameters from each block are collected from the simulation to be used as inputs for the estimation model. The model returns the number of operations, and the operations if not defined in Section III are assumed to be a FLOP, i.e., an addition and a multiplication. The datatypes of Blocks A, G, scrambling and modulation inputs, from Block B, and descrambling input, from Block G, are assumed to be integer or logical while the other algorithms and blocks are assumed to have a double type inputs. Regarding the Block H, the number of variable nodes connected to a check node, the number of check nodes connected to a variable node and the number of iterations is assumed to be a constant, for sake of simplicity for this initial study.

Fig. 1 is the graphic representation of the results obtained from the Measurements and Model estimation for one slot with a single codeword, 10 db of SNR, 15 KHz subcarrier spacing, 16 quadrature amplitude modulation (QAM), coding rate equal to 490/1024, four antennas on both transmitter and receiver, and two layers. The value considered for κ is $10^{-25} J \cdot s^2$, the same value used in Hao et al. [15], and f_p equal to 2.1 GHz. The vertical axis is in logarithmic scale to allow the visualization of all the blocks. Each block has two bars, one for the Model, in blue, and other for the Measurements, in orange. In the blocks A, E, F, and H, the model presents an overestimation of the amount of energy consumed, compared to the simulations, while in the blocks B, C, D, and G, the model presents an underestimation of the energy consumed.

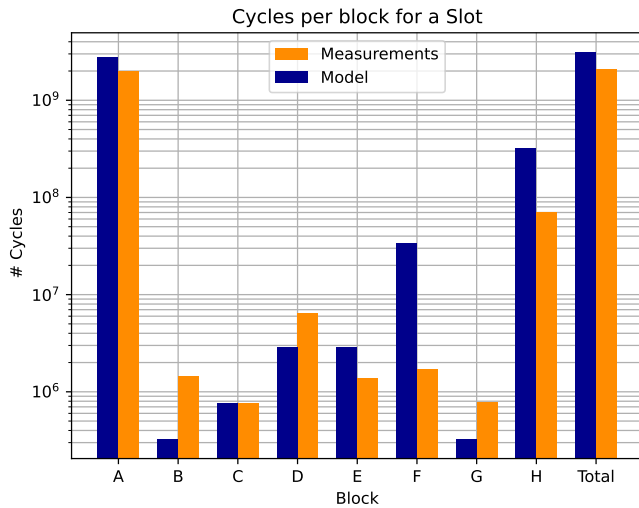


Figure 1. Number of cycles per block and the total number for a single slot transmission on downlink.

The results for the energy estimation by the model, compared to the simulations results obtained from MATLAB, are similar (discrepancies are explainable). The blocks with large matrix multiplication, like in blocks A and F, can be overestimated due to the model used for matrix multiplication, a schoolbook based approach, that can be too greedy, specially in the cases of sparse matrices, like the base graph matrix for channel coding, while MATLAB uses optimized algorithms. The same happens for the matrix inversion. In other blocks like B and G, the underestimation can be explained by the fact that while the model assume that most of its energy consumption comes from the RF chain, and so, does not consider it, while the measurements, in MATLAB, does compute all the modulation operations, and so, the validations results contains both RF and BBU parts.

Figs. 2 and 3 are the results of results obtained in terms of cycles per bit by changing only the modulation to QPSK, 16 QAM and 64 QAM for model and measurements, respectively. Once the total number of cycles per block is acquired, it is divided by the number of bits sent over the transmission. In both Figs, is possible to see that the higher the modulation,

the less the number of cycles required to process and transmit them, in accord which is expected. However, in the model, for Block A, the same behavior is not seen, which requires further investigations.

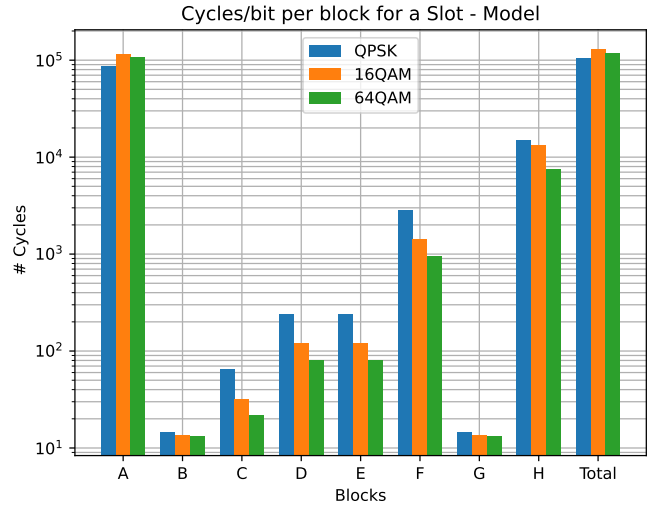


Figure 2. Number of cycles per bit estimated by the model for the blocks and total number of cycles of modulations QPSK, 16QAM, and 64QAM for a single slot transmission on downlink.

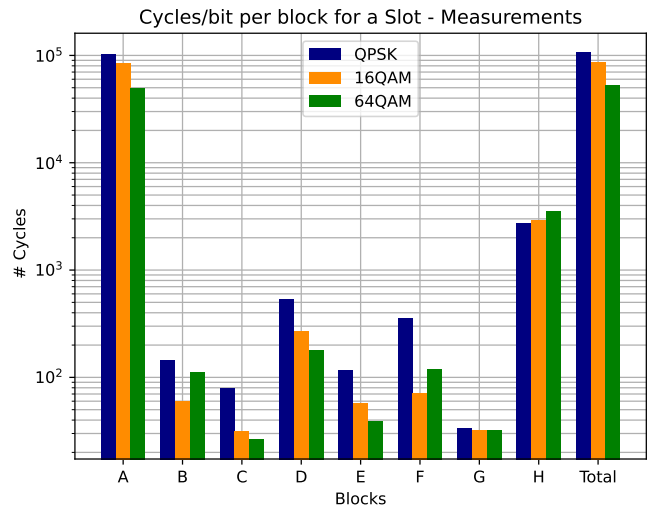


Figure 3. Number of cycles per bit estimated by the measurements for the blocks and total number of cycles of modulations QPSK, 16QAM, and 64QAM for a single slot transmission on downlink.

As the available results are in a micro-scale, i.e., at a slot level, a direct comparison with other methods cannot be established up to now. The results indicate that the model is globally in agreement with the simulations, but we need to take further optimized algorithms (e.g optimized matrix operation algorithms) into account. The model presents a first step towards a method for smaller granularity that can be extended for multiple applications and different contexts, hence opening the possibility to compare the real impact of different

algorithmic and architectural choices in the implementation of 5G.

V. CONCLUSION

By proposing a method based on the number and type of computational operations performed at the 5G PHY-layer for a downlink transmission and reception, we address the development of a versatile energy model applied to 5G to estimate the RAN specific energy consumption encompassing both the mobile terminal and the PHY-layer part of the base station. We design a first version of the model based on eight blocks, whose implementation based complexity estimations are similar to the operations based model. Further enhancements on the model are necessary for the application of this model in a larger scale and different contexts.

REFERENCES

- [1] P. Jonsson, A. Lundvall, R. Möller, S. Carson, and S. Davies, "Ericsson mobility report," Ericsson, Tech. Rep., nov 2022.
- [2] Nokia, *5G network energy efficiency Massive capacity boost with flat energy consumption*, 2016.
- [3] G. Auer, V. Giannini, C. Desset, I. Godor, P. Skillermark, M. Olsson, M. A. Imran, D. Sabella, M. J. Gonzalez, O. Blume *et al.*, "How much energy is needed to run a wireless network?" *IEEE wireless communications*, vol. 18, no. 5, pp. 40–49, 2011.
- [4] C. Desset, B. Debaillie, V. Giannini, A. Fehske, G. Auer, H. Holtkamp, W. Wajda, D. Sabella, F. Richter, M. J. Gonzalez *et al.*, "Flexible power modeling of lte base stations," in *2012 IEEE wireless communications and networking conference (WCNC)*. IEEE, 2012, pp. 2858–2862.
- [5] M. Yan, C. A. Chan, A. F. Gygax, J. Yan, L. Campbell, A. Nirmalathas, and C. Leckie, "Modeling the total energy consumption of mobile network services and applications," *Energies*, vol. 12, no. 1, p. 184, 2019.
- [6] D. López-Pérez, A. De Domenico, N. Piovesan, G. Xinli, H. Bao, S. Qitao, and M. Debbah, "A survey on 5g radio access network energy efficiency: Massive mimo, lean carrier design, sleep modes, and machine learning," *IEEE Communications Surveys & Tutorials*, vol. 24, no. 1, pp. 653–697, 2022.
- [7] L. Williams, B. K. Sovacool, and T. J. Foxon, "The energy use implications of 5g: Reviewing whole network operational energy, embodied energy, and indirect effects," *Renewable and Sustainable Energy Reviews*, vol. 157, p. 112033, 2022.
- [8] L. M. Larsen, H. L. Christiansen, S. Ruepp, and M. S. Berger, "Toward greener 5g and beyond radio access networks—a survey," *IEEE Open Journal of the Communications Society*, vol. 4, pp. 768–797, 2023.
- [9] D. Xu, A. Zhou, X. Zhang, G. Wang, X. Liu, C. An, Y. Shi, L. Liu, and H. Ma, "Understanding operational 5g: A first measurement study on its coverage, performance and energy consumption," in *Proceedings of the Annual conference of the ACM Special Interest Group on Data Communication on the applications, technologies, architectures, and protocols for computer communication*, 2020, pp. 479–494.
- [10] A. Narayanan, X. Zhang, R. Zhu, A. Hassan, S. Jin, X. Zhu, X. Zhang, D. Rybkin, Z. Yang, Z. M. Mao *et al.*, "A variegated look at 5g in the wild: performance, power, and qoe implications," in *Proceedings of the 2021 ACM SIGCOMM 2021 Conference*, 2021, pp. 610–625.
- [11] S. Tombaz, P. Frenger, F. Athley, E. Semaan, C. Tidestav, and A. Furuskar, "Energy performance of 5g-nx wireless access utilizing massive beamforming and an ultra-lean system design," in *2015 IEEE Global Communications Conference (GLOBECOM)*. IEEE, 2015, pp. 1–7.
- [12] G. Yu, Q. Chen, R. Yin, H. Zhang, and G. Y. Li, "Joint downlink and uplink resource allocation for energy-efficient carrier aggregation," *IEEE Transactions on Wireless Communications*, vol. 14, no. 6, pp. 3207–3218, 2015.
- [13] Y. Fu, M. D. Soltani, H. Alshaer, C.-X. Wang, M. Safari, S. McLaughlin, and H. Haas, "End-to-end energy efficiency evaluation for b5g ultra dense networks," in *2020 IEEE 91st Vehicular Technology Conference (VTC2020-Spring)*. IEEE, 2020, pp. 1–6.
- [14] A. Fog, "Optimization manual 4 instruction tables," *Copenhagen University College of Engineering, Software Optimization Resources*, <http://www.agner.org/optimize> (Jan. 5, 2010),(1996-2009), pp. 1–154, 1996.
- [15] Y. Hao, M. Chen, L. Hu, M. S. Hossain, and A. Ghoneim, "Energy efficient task caching and offloading for mobile edge computing," *Ieee access*, vol. 6, pp. 11 365–11 373, 2018.
- [16] I. Barhumi, G. Leus, and M. Moonen, "Optimal training design for mimo ofdm systems in mobile wireless channels," *IEEE Transactions on signal processing*, vol. 51, no. 6, pp. 1615–1624, 2003.